?. Circular Receptive Field Structures for Flow Analysis and Heading Detection

Jaap A. Beintema*, Albert V. van den Berg*, Markus Lappe§

* Functionele Neurobiologie, Universiteit Utrecht, Utrecht, The Netherlands
§ Allgemeine Psychologie, Westf. Wilhelms-Universität Münster, Münster; and
Allgemeine Zoölogie & Neurobiologie, Ruhr-Universität Bochum, Bochum, Germany

I. INTRODUCTION

Recent years have brought forward different models on how the brain might encode heading from optic flow. Neurons in these models can encode heading for a variety of self-motion conditions, while responding to optic flow stimuli similarly as found in electrophysiological studies. Yet, little attention has been given to the receptive field structure of neurons that integrate local motion signals to analyse the optic flow. Intuitively, radial structures might seem suited for the task of heading detection, since pure observer translation causes flow to eminate from the point of heading (Figure 1a). However, rotational flow (Figure 1b) during simultaneous eye rotation can cause the retinal flow to be shifted away from the heading (Figure 1c). Moreover, variation in point distances with respect to the translating eye results in retinal motion differences, called motion parallax, that can cause the flow during eye rotation to deviate even more from being purely radial. This poses the question what would be the optimal receptive field structure to deal with complex flow fields for retrieving heading.

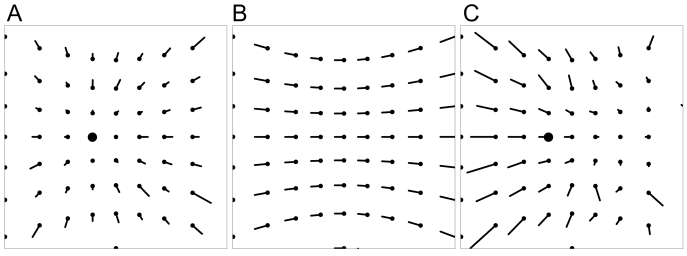

Figure 1. Flow during a) observer translation through a 3D-cloud of dots, headed 10 degrees towards the left (filled circle), during b) observer rotation about the vertical towards the right, and during c) the combination of both. The dots indicate the start of motion vectors.

Research on neural mechanisms has focussed on a number of cortical areas that contain cells responsive to optic flow, such as area MST (human V5a) but also areas beyond such as VIP (Colby, Duhamel & Goldberg, 1993) or 7a (Read & Siegel, 1997). MST neurons typically have large receptive fields that cover more than a quarter of the visual field, and respond well to complex motion patterns, such as expanding/contracting motion, clock-wise/counterclockwise rotation (Tanaka, Fukada & Saito, 1989; Tanaka & Saito, 1989), or combinations of rotation and expansion (Graziano, Andersen & Snowden, 1994). Importantly, MST cells seem systematically tuned to the location of foci of expansion or rotation (Duffy & Wurtz, 1995; Lappe, Bremmer & Pekel, 1996). Convincing evidence for MST's involvement in heading perception has been found from the covariation of MST activity with the heading responses of trained monkeys (Britten & van Wezel, 1998). MST cells acquire their selectivity to optic flow by integrating signals from local motion sensors, found in area MT (human V5). MT neurons have smaller RFs and typically respond to motion in one particular direction at a particular speed (see review van Wezel & Britten, 2002). Still, relatively little is known about the organisation of the MT neurons that form the receptive field (RF) of an MST cell tuned for heading.

Several schemes have been proposed to recover heading from optic flow in the presence of rotational flow (see review Lappe, 2000). Intuitively, one might think that detectors for expansion would be ideal for detecting heading. Radial receptive fields are for example assumed by differential motion models that take local motion differences as to remove the effect of rotation (Longuet-Higgins & Prazdny 1980; Hildreth 1992; Rieger & Lawton 1985), for the remaining motion parallax vector field radiates from the heading direction. Indeed, such approaches find some physiological support, as MT cells have been found that respond well to motion differences in their center and surround receptive field (Allman, Miezin & McGuinness, 1985), and a heading detection scheme based on motion-opponent cells seems feasible (Royden, 1997). The analysis of the remaining differential motion vectors could be realised by pure translation detectors with radial receptive fields (Hatsopoulos & Warren, 1991). But, differential motion parallax models can only partly explain human psychophysics on heading perception. Importantly, these models fail to detect heading in the absence of depth differences, whereas humans still correctly can judge heading by relying on extra-retinal rotation signals (Royden, Banks & Crowell, 1992), or given a sufficiently large field of view (Grigo & Lappe, 1999).

Yet, the last decade has brought forward a number of physiologically inspired models that detect heading in the presence of eye rotation for a variety of conditions and are able to simulate response properties of MST cells (Beintema & van den Berg, 1998; Lappe & Rauschecker, 1993b; Perrone & Stone, 1994). As these models deal with eye rotation at the level beyond local motion detection, the receptive field of their MST-like neurons must differ from purely radial.

So far, the receptive field structure using small field stimuli has only been roughly been probed (Duffy & Wurtz, 1991b). Those results give little support for simple RF structures such as radial motion or uni-circular motion (clockwise or counterclockwise rotation). Another intriguing question is why a large proportion of MST cells respond to clockwise or counterclockwise rotation (Duffy & Wurtz 1991, a,b; Lappe et al., 1996; Tanaka & Saito, 1989) at rotation speeds up to 80 deg/s not usually experienced in daily life.

These observations inspired us to examine the receptive fields predicted by three physiologically inspired models. In the following, we first introduce the RF structure assumed in templates of the velocity gain model (Beintema & van den Berg, 1998). Then we present an analysis of the RF structures that emerge under different restrictions of the population model (Lappe & Rauschecker, 1993b). Finally, we consider the effective RF structure of the template model (Perrone & Stone, 1994). Despite the different approaches, a striking similarity is found. The preferred motion driving the neurons turns out to be directed always along circles centered on the neuron's preferred heading, thus perpendicular to the expected radial flow. Moreover, we find similarities and differences in the substructures, such as bi-circularity and motion-opponency, which might reveal different strategies on how the visual system copes with eye rotation.

II. VELOCITY GAIN FIELD MODEL

The velocity gain field model by Beintema and van den Berg (1998) is based on the templates approach (Perrone, 1992; Perrone & Stone, 1994). That approach aims to find the best matching template in a set of motion templates tuned to different ego-motions. Each template evaluates the evidence for a global match with its preferred flow by summating evidence for local matches across different parts in the visual field. How these local comparisons are done is not trivial, but by appropriate selection of the motion sensors at a specific retinal location, templates can be constructed that respond maximally only to flow corresponding to a particular heading in combination with a particular ego-rotation, independent of the distances of points.

The velocity gain field model differs from the template approach in two important ways. First of all, invariance to rotation is obtained using explicit estimates of rotation, allowing the use of rate-coded extra-retinal signals and reducing the dimensions of templates needed to represent all possible combinations of heading direction and ego-rotations. Secondly, as to construct templates insensitive to the translational velocity or distances of points, the RF structure of templates in the velocity gain field model was assumed constrained in an explicit non-radial way. These two steps in achieving invariance to parameters other than heading will be explained below.

II.I Basic scheme in Velocity Gain Field model

The basic scheme used by the velocity gain field model is given in Figure 2. Heading is encoded by a collection of templates, each with their own preferred heading $\mathbf{t}$ and output response $H_{\mathbf{t}}$. The input to each template $H_{\mathbf{t}}$ is a bundle of templates sharing the same preferred heading $\mathbf{t}$, but having different preferred rotations. In principle, three pairs of templates tuned the same heading, each pair having opposite preferred rotation ($\pm$) about one of the cardinal axes of rotation, are sufficient to make the template $H_{\mathbf{t}}$ invariant to rotation magnitudes up to [] (Beintema & van den Berg, 1998).

First of all, invariance for rotation about a given axis is obtained when the template activity $H_{\mathbf{t}}$ equals the activity of a template that shifts its preferred rotation dynamically as much as the actual rotation []. Generally, a shift of a Gaussian tuning function can be accomplished by a Taylor series, with first and higher order Gaussian derivatives, each term appropriately scaled by first and higher order powers of the desired shift. The response of a template $O_{\mathbf{t},R+\Delta R}$, shifted in its preferred rotation by an amount [], is given to first approximation by $O_{\mathbf{t}} + \Delta R \cdot \partial O_{\mathbf{t}} / \partial R$ (Beintema & van den Berg, 1998). Note, the signal [] can be an extra-retinal or a visual estimate of rotation velocity.

The idea of dynamically shifting templates can also be understood in terms of compensating activity. The activity $H_{\mathbf{t}}$ needs to be corrected for a change in the activity of the pure translation template $O_{\mathbf{t}}$ in case of rotational flow. Simply subtracting the rate-coded rotation velocity signal [] would not suffice to compensate. For this, [] needs to be multiplied by a visual activity that tells how $O_{\mathbf{t}}$ changes with a change in rotational flow, i.e. the so called derivative template $\partial O / \partial R$. Since the compensation term $\Delta R \cdot \partial O / \partial R$ has the property of being gain-modulated by the extra-retinal velocity signal, this approach has been called the velocity gain field model, analogue to eye position gain fields as reported in area 7a (Andersen, Essick & Siegel, 1985).

The model does not require an explicit representation of the subunits as suggested in the scheme. The output of the derivative template $\partial O / \partial R$ can be approximated by the difference activity of two templates tuned to the same heading, but opposite rotation ($O_{\mathbf{t},\pm\Delta R}$). Alternatively, however, the derivative template could also have been computed directly by summing local difference signals from pairs of motion sensors, each sensor of the pair having equal but oppositely directed preferred motion (Beintema & van den Berg, 1998). Likewise, the pure translation template $O_{\mathbf{t}}$, tuned to heading but zero rotation, need not be directly computed, but could also be derived from the average response of two rotation-tuned templates with opposite preferred rotation directions, hence the dotted lines feeding the template $O_{\mathbf{t}}$.

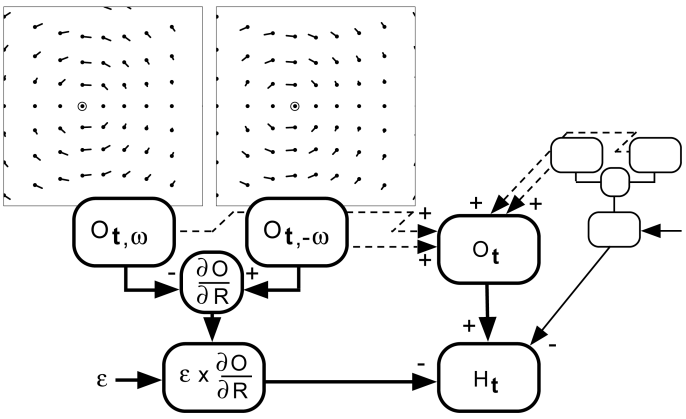

Figure 2. Basic components in the velocity gain field model. The RF structure of typical units, tuned to heading (open circle) and simultaneous left- or rightward rotation about the vertical, is bi-circular. Vectors indicate the preferred direction and velocity of the input motion sensors.

To explain the second step of acquiring insensitivity to the distances of points or the translational velocity, assume a polar coordinate system centered on the direction of heading. Then, the retinal flow can be split into its radial and its circular component (Figure 3). The radial component contains the translational component of the flow, and will vary with translational speed or point distances. The circular component, in contrast, only depends on the rotational component of the flow. This observation leads to the assumption implemented in the velocity gain field model that templates should only measure the flow along circles centered on the point of preferred heading. By assuming such *circular* RF structure, the template strongly reduces sensitivity to variations in depth structure or the translational speed, while preserving its tuning to heading direction and the rotational component of flow (Beintema & van den Berg, 1998).

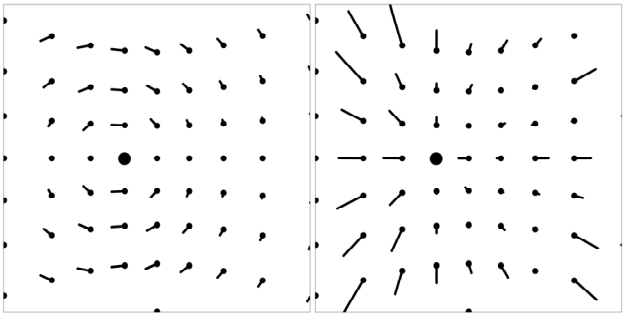

Figure 3. The heading-centered circular (left) and radial (right) component of the flow during combined translation and rotation as in Figure 1c.

II.II Receptive Fields in Velocity Gain Field model

Given templates measure only motion along circles centered on the template's preferred heading, what does the RF structure look like for the units in the velocity gain field model? The RF of a typical pair of templates tuned to heading and opposite rotations about the vertical axis is shown in Figure 2. Note, their preferred structure does not resemble *uni-circular* flow, because the directions of preferred motion vectors reverse across the meridian through the preferred heading and perpendicular to the preferred rotation axis (in this case the horizontal meridian). It is for this reason that the structure has been coined *bi-circular* (van den Berg, Beintema & Frens, 2001). Another characteristic of the bi-circular structure is the gradient in motion magnitude along the circle, vanishing at points along the meridian that is perpendicular to the rotation axis. Generally, any unit tuned to rotation about an axis perpendicular to the heading will have a bi-circular structure, modulo a clockwise rotation. For rotation about the horizontal axis, for instance, the bi-circular pattern will be 90 degrees rotated about the heading point.

A similar RF arises if the derivative template is not computed from the difference activity of a pair of rotation-tuned templates, but computed directly. In that case, the RF is expected to be closely related to that of the bi-circular RF. Since the derivative template then is computed from the local difference of the outputs of two motion template, the RF is represented by the superposition of the two RFs. Interestingly, the receptive field then consists of pairs of motion sensors with opponent-motion directions along circles centered on the preferred heading, and with magnitude gradient as found for the bi-circular RF structure.

An even more counterintuitive RF structure is expected for the pure translation template $O_{\mathbf{t}}$, whose output is compensated by the rotation-tuned units. This template is maximally excited when presented with zero motion along its preferred motion directions, i.e. along circles centered on the preferred heading. Such local responses could be accomplished by MT cells that respond maximally to zero-motion while being inhibited by motion in their preferred or anti-preferred direction. Alternatively, as stated before, a pure translation tuned template might also sum the activities of template pairs with opposite preferred rotations but identical heading. Stimulated with flow corresponding to the preferred heading and zero rotation, the output of each rotation-tuned template is balanced by its counterpart with opposite preferred rotation, so that the mean activity will peak at the desired preferred heading. In this case, the predicted RF structure locally consists of motion-opponent pairs as well. But, in contrast to the derivative template, these motion-opponent pairs do not compute the local difference activity of such pairs, but their sum.

III. POPULATION MODEL

The population model by Lappe and Rauschecker (1993b) takes a very different approach to encode heading. The model is an implementation of the subspace algorithm by Heeger and Jepson (1992b) that sets the connection strengths and preferred directions of local motion inputs to heading-specific flow units.

First, we recapitulate the basics of the subspace algorithm, and its neural implementation. Then, we analytically derive the RF structure. Different versions of the model have been proposed (Lappe & Rauschecker, 1995). In the restricted version of the model, the eye movements are assumed to be limited to tracking a stationary point in the scene during the observer translation, without torsion about the line of sight. In the non-restricted version, eye movements are assumed to be independent of the heading, and free to rotate about any axis. The effect of both constraints we shall analyse. Part of the results for restricted eye movements have been published in short form (Beintema, van den Berg & Lappe, 2001). Here, we present the mathematics and the extension to unrestricted eye movements as well.

III.I. Subspace Algorithm

The subspace algorithm resolves the unknown translation direction Π from optic flow vectors without requiring knowledge of the three-dimensional rotation vector Π and depths Z_i of m points. In this approach, each flow vector at a given image location (x,y) is written as

$$\Pi(x,y) = \frac{1}{Z(x,y)}\mathbf{A}(x,y) + \mathbf{B}(x,y)\Pi \tag{0.1}$$

with the matrices $\mathbf{A}$ and $\mathbf{B}$ depending on image positions (x,y) and focal length f (Heeger & Jepson 1992b):

$$\mathbf{A}(x,y) = \begin{bmatrix} -f & 0 & x \\ 0 & -f & y \end{bmatrix} \text{ and } \mathbf{B}(x,y) = \begin{bmatrix} xy/f & -f - x^2/f & y \\ f + y^2/f & -xy/f & -x \end{bmatrix} \tag{0.2}$$

By putting all flow components sequentially in a generalised flow vector Π^t, the $2m$ flow equations can be written in matrix form by $\Pi^t = \mathbf{C}(\mathbf{T}) \cdot \mathbf{q}$. Here, $\mathbf{C}(\mathbf{T})$ is a $2m \times (m+3)$ matrix depending on n image positions and the translation vector $\mathbf{T}$

$$\mathbf{C}(\mathbf{T}) = \begin{bmatrix} \mathbf{A}(x_1,y_1)\mathbf{T} & \cdots & 0 & \mathbf{B}(x_1,y_1) & \\ \vdots & \ddots & \vdots & \mathbf{B}(x_2,y_2) & \\ 0 & 0 & \mathbf{A}(x_m,y_m) & \mathbf{B}(x_m,y_m) & \end{bmatrix} \tag{0.3}$$

and $\mathbf{q}$ is a $(m+3)$-dimensional vector containing the m unknown inverse depths and the three-dimensional rotation vector. The unknown heading $\mathbf{T}_j$ can be solved least squares by minimizing a residual function $R(\mathbf{T}_j) = \left\| \quad ^t \quad \mathbf{C}(\mathbf{T}_j) \cdot \mathbf{q} \right\|^2$. This is equivalent to finding the translation vector $\mathbf{T}_j$ that minimizes

$$R(\mathbf{T}_j) = \left\| \quad ^t \mathbf{C}^{\perp}(\mathbf{T}_j) \right\|^2 \tag{0.4}$$

where $\mathbf{C}^{\perp}(\mathbf{T}_j)$ is the orthogonal complement of $\mathbf{C}(\mathbf{T}_j)$ (Heeger & Jepson, 1992b). For the general case of unrestricted eye movements, the columns of $\mathbf{C}(\mathbf{T}_j)$ form a basis of an $m+3$ subspace of the ^{2m}, called the range of $\mathbf{C}(\mathbf{T}_j)$. The orthogonal complement is a matrix that spans the remaining $(2m \quad (m+3))$-dimensional subspace of $\mathbf{C}(\mathbf{T}_j)$. Its columns form the nullspace of the $\mathbf{C}(\mathbf{T}_j)$. Each column is a nullvector and is orthogonal to every row vector of $\mathbf{C}(\mathbf{T}_j)$ (Heeger & Jepson, 1992b).

III.II. Neural Implementation of the Subspace Algorithm

Lappe and Rauschecker (1993b) implemented the subspace algorithm in a neural network to compute a priori the connections between MT and MST neurons. Their model approach starts by representing the measured flow vector $\quad_i$ by the activity of n local motion sensors s_{ik} with MT-like direction tuning and velocity tuning functions so that $\quad_i = \quad_{k=1}^{n} s_{ik}\mathbf{e}_{ik}$. We represent the motion vector by 4 mutually perpendicular preferred motion sensors in directions $\mathbf{e}_{ik}$ with cosine-like direction tuning and linear velocity tuning (Lappe & Rauschecker, 1993b, 1995). The measured motion vector could equally well be represented by an extended set of activities based on motion sensors with tuning to specific speeds (Lappe, 1998) without changing our results.

The motion signals from different locations i are collected by second layer neurons that compute the residual function. Their output is a sigmoidal function g of the weighted sum of the inputs s_{ik}

$$u_{jl} = g(\sum_{i=1}^{m} \sum_{k=1}^{n} J_{jl,ik} s_{ik} - \theta) \tag{0.5}$$

where $J_{jl,ik}$ is the synaptic strength between the l-th output neuron in second layer population representing heading direction $\mathbf{T}_j$ and the k-th input neuron in the first layer representing the optic flow vector Ω_i.

According to the subspace algorithm, the residual function is minimized when all the measured flow vectors, described by vector Ω^t, are perpendicular to the l-th column of $\mathbf{C}^{\perp}(\mathbf{T}_j)$. By requiring the input to the neuron to be $\Omega^t \mathbf{C}_l^{\perp}(\mathbf{T}_j)$, the synaptic strength for a single second layer neuron will need to be (Eq. 20 in Lappe, 1998):

$$J_{jl,ik} = e_{ik}^t \frac{C_{l,2i-1}^{\perp}(\mathbf{T}_j)}{\left\| C_{l,2i}^{\perp}(\mathbf{T}_j) \right\|} \tag{0.6}$$

Finally, the population model computes the residual function in a distributed way, partitioning the residual function $R(\mathbf{T}_j)$ into a sum of subresidues, each computed by the l-th neuron. Heading is then represented by the sum of neurons responses $U_j = \sum_l u_{jl}$. Each l-th neuron, tuned to the correct heading direction, exhibits a sigmoid surface with a rising ridge (not a Gaussian blob) as function of the two-dimensional heading. Although each l-th neuron may have a ridge of different orientation, its position is constrained by the algorithm to pass through the preferred heading $\mathbf{T}_j$. Thus, the population sum activity U_j will peak at the preferred heading. To help ensure that a peak is created, each sigmoid function in Eq. 5 is slightly offset by θ (Lappe & Rauschecker, 1993b).

III.III. Receptive Fields in Population Model

What set of preferred motion directions and connections strengths would be optimal to ensure that the residual function is minimized when presented with the correct heading? According to Eq. 6, the synaptic strengths at each location are given by the subvector in the l-th column of $\mathbf{C}^{\perp}(\mathbf{T}_j)$. We can map the preferred motion $\mathbf{v}_{jl,i}$ by the vector sum of responses to equal stimulation in the $n = 4$ motion sensor directions.

$$\mathbf{v}_{jl,i} = \sum_{k=1}^{n} J_{jl,ik}\mathbf{e}_{ik} = \begin{bmatrix} C^{\perp}_{l,2i-1}(\mathbf{T}_j) \\ C^{\perp}_{l,2i}(\mathbf{T}_j) \end{bmatrix} \tag{0.7}$$

Thus, we see that the preferred motion input (motion direction and synaptic strength) are directly given by the two-dimensional subvectors (by the orientation and length, respectively) that make up the orthogonal complement. The population model divides the labour of computing the residual function over different neurons u_{jl} that can have arbitrary number of inputs. By taking the minimum of flow inputs required to compute the orthogonal complement, we can reduce the matrix $\mathbf{C}(\mathbf{T}_j)$ so that its orthogonal complement can be solved analytically. Note, the set of motion vectors that is found this way is forms a subset of the receptive field encoding a specific heading. The smallest number of flow inputs for which the orthogonal component can be computed given unrestricted eye movements is $m = 4$. For this case, $\mathbf{C}^{\perp}(\mathbf{T}_j)$ consists of a single column $l = 1$ with 8 elements. For restricted eye movements that are constrained to null the flow at the center of the image, i.e. stabilize gaze on the object at the fovea, without rotation about the line of sight, the rotation Ω can be expressed in terms of $\mathbf{T}$ and the fixation distance Z_f. This assumption reduces $\mathbf{C}(\mathbf{T}_j)$ to a $2m \times (m+1)$-dimensional matrix, and $\mathbf{C}^{\perp}(\mathbf{T}_j)$ to a $(m-1) \times 2m$-dimensional matrix (Lappe & Rauschecker, 1993a). Then, for $m = 2$ flow vectors, the orthogonal complement $\mathbf{C}^{\perp}(\mathbf{T}_j)$ consists of only a single column ($l = 1$) with length 4 and can be exactly solved. We will first analyse the RF structure for the simplest case of tracking eye movements and two input vectors. Then, we analyse results for the case of unconstrained eye movements and arbitrary numbers of input vectors.

III.IV. Case of Restricted Eye Movements

First, we compute the matrix $\mathbf{C}(\mathbf{T}_j)$ for restricted eye movements. We can choose the preferred heading $\mathbf{T}_j$ to be horizontal ($T_y = 0$) without loss of generality because of symmetry in the xy-plane. Furthermore, we can also set T_z and the focal distance f to unity, so that the heading vector intersects the image plane at the point $f(T_x/T_z, T_y/T_z) = (T_x, 0)$. Then $\mathbf{C}(\mathbf{T}_j)$ becomes

$$\mathbf{C}(\mathbf{T}_j) = \begin{bmatrix} -T_x + x_1 & 0 & T_x(1+ x_1^2) / Z_f \\ y_1 & 0 & T_x x_1 y_1 / Z_f \\ 0 & -T_x + x_2 & T_x(1 + x_2^2) / Z_f \\ 0 & y_2 & T_x x_2 y_2 / Z_f \end{bmatrix} \tag{0.8}$$

The orthogonal complement was computed analytically. For this we used Mathematica to solve the nullspace of the inverted matrix of $\mathbf{C}(\mathbf{T}_j)$. The result presented here is written short by transforming the image coordinates to a system centered on the projection of the translation vector (T_x,T_y) (i.e. $\tilde{x}_i = x_i - T_x$). Then, $\mathbf{C}^{\perp}(\mathbf{T}_j)$ becomes

$$\mathbf{C}^{\perp}(\mathbf{T}_j) = \begin{bmatrix} \tilde{y}_2 / \tilde{x}_2 \dfrac{1+T_x(T_x+\tilde{x}_2)}{1+T_x(T_x+\tilde{x}_1)} \\ -\tilde{y}_2 \tilde{x}_1 / (\tilde{y}_1 \tilde{x}_2) \dfrac{1+T_x(T_x+\tilde{x}_2)}{1+T_x(T_x+\tilde{x}_1)} \\ -\tilde{y}_2 / \tilde{x}_2 \\ 1 \end{bmatrix} \tag{0.9}$$

III.IV.I. Circular RF Structures

An example of the RF structure that emerges for arbitrarily chosen pairs of neurons u_{jl}, whose summed responses encode the preferred heading, is given in Figure 4. Most noticeably, the RF structure appears to be organised circularly, and centered on the preferred heading. This would mean that the preferred motion vector $\mathbf{v}_i$ is oriented perpendicular to the vector that radiates from the preferred heading and passes through the location of the motion vector $(\tilde{x}_i,\tilde{y}_i)$. Indeed, as can be seen from Eq. 9, $\mathbf{v}_i \cdot (\tilde{x}_i,\tilde{y}_i) = 0$ for $i = 1$ and $i = 2$.

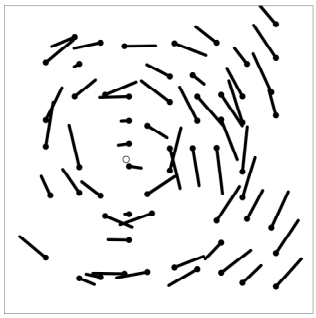

Figure 4. Examples of RF structure of 30 pairs, each pair being input to an u_{jl} neuron with preferred heading 10 degrees towards the left (open circle).

III.IV.II. Motion Opponent RF Structures

We then analysed in more detail how the preferred motion directions and magnitudes relate to the relative position of motion inputs. First of all, we found that for pairs of motion sensors at nearby locations, the vectors of each pair tend to be opponent (pair A in Figure 5). Indeed, for two motion inputs located infinitely close to each other ($\tilde{x}_2 = \tilde{x}_1$ and $\tilde{y}_2 = \tilde{y}_1$), the orthogonal complement simplifies to $\mathbf{C}^{\perp}(\mathbf{T}_j) = (\tilde{y}_1 / \tilde{x}_1, -1, -\tilde{y}_1 / \tilde{x}_1, 1)^t$. Denoting the angular velocity of a vector $\mathbf{v}$ along the circle by scalar v, we find the ratio of preferred angular velocities is ($v_1 / v_2 = -1$). This proofs the preferred directions in this case are always opposite and of equal magnitude.

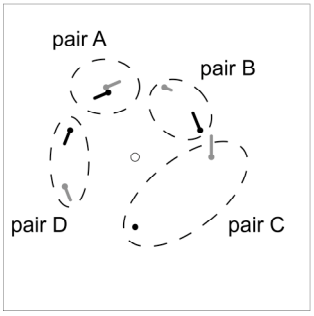

Figure 5. Examples of local direction preferences in a RF from a population of 4 motion pairs (A-D). The MST neuron encodes heading 10 degrees towards the left (open circle).

To describe the preferred motion for pairs of motion sensors at different locations, let us define the image location of points in a polar coordinate system centered on the preferred heading. So, points on the same circle have different polar angles, but constant eccentricity with respect to the heading.

We exemplify our observations by a few pairs of motion input in Figure 5. First of all, the difference between motion magnitudes increases sinusoidally with the polar angle difference between the two points (compare pair A, B and C). Secondly, consider the meridian through the fixation and heading point. The preferred motion directions are opponent if the pair is located on the same side with respect to that meridian (pair A, B, C).

III.IV.III. Bi-circular RF Structures

We also found other interesting substructures under certain constraints on the locations of motion inputs. The preferred motion directions are uni-directional if the pair is split across the meridian through fixation and heading (Figure 5, pair D). Moreover the magnitudes are equal for positions that mirror in the meridian (pair D). Also, eccentricity with respect to the heading had no influence on the preferred motion vectors. In principle, this would allow the construction of a uni-circular RF. Interestingly, we found that if pairs of motion sensors have their partners at image locations 90 degrees rotated about the heading point, a magnitude gradient appears, and a RF structure can be constructed (Figure 6) that has great similarity to bi-circular RF pattern predicted by the velocity gain field model (Figure 2).

Figure 6. Distribution of pairs of neurons with preferred heading 10 deg left, arranged to make bi-circular RF.

III.V. Case of Unrestricted Eye Movements

We then computed analytically the orthogonal complement for the minimum number of required motion inputs in case of unrestricted eye movements ($m = 4$). Again, we find only circular RFs structures. We analysed the preferred motion magnitudes and directions for various spatial arrangements. In Figure 7 we plotted three possible spatial arrangements. In contrast to results for restricted eye movements, none of these structures appeared to fit a uni-circular structure, nor the bi-directionality and magnitude

gradient expected for a bi-circular RF structure. We do find an influence of eccentricity, and a strong degree of motion-opponency. In the special case when pairs of motion vectors were located at exactly the same position, each pair turns out to have equal but opposite preferred motions (Figure 7c).

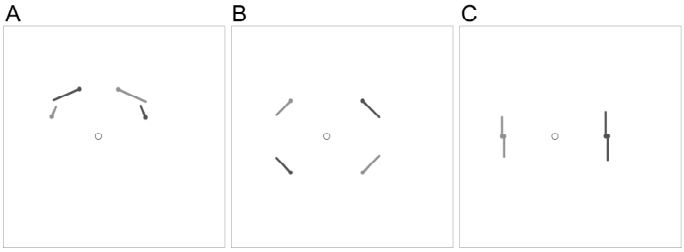

Figure 7. Preferred motion vectors for neuron u_{jl} in case of unrestricted eye movements given four motion inputs. The motion inputs are chosen on a circle centered on the heading direction (open circle) and separated by 45 (a), 90 (b) and 180 degree (c).

III.V.I. General solution

Simulations showed the result of circularity applied to any number of vectors inputs. A similar result can actually be found in the proof of the existence and uniqueness of solutions to the subalgorithm (Heeger & Jepson, 1990). From Eq. 3, one can see that any nullvector of $\mathbf{C}(\mathbf{T}_j)$ must be a linear summation of m vectors $\Box_i$ of the following form:

$$\Box_i = (0,0,0,0,\cdots,\Box_{ix},\Box_{iy},\cdots,0,0) \tag{0.10}$$

These vectors are perpendicular to the first m columns of $\mathbf{C}(\mathbf{T}_j)$ and have two non-zero elements given by $\Box_i \cdot \mathbf{A}(x_i, y_i)\mathbf{T}$. Substituting $(T_y = 0, T_z = 1, f = 1)$ for $\mathbf{A}$ in Eq. 2, the elements of each vector are related by:

$$\Box_{iy} / \Box_{ix} = \frac{x_i \Box T_x}{\Box y_i} = \frac{\tilde{x}_i}{\Box \tilde{y}_i} \tag{0.11}$$

As each $\Box_i$ is oriented along a circle centered on the heading point, any weighted combination $\Box_{i=1}^{m} c_i \Box_i$ will be oriented circularly as well. The weights c_i follow from the requirement of rotation invariance, i.e. the weighted vectorsum must also be perpendicular to the remaining columns of $\mathbf{C}(\mathbf{T}_j)$ made out of $\mathbf{B}$ matrices (Eq. 2).

When the number of flow vector inputs is larger than the minimum required

(2 for tracking eye movements, 4 for unrestricted eye movements), the problem of computing the nullspace of $\mathbf{C}(\mathbf{T}_j)$ become underdetermined, so that only a continuum of possible solutions exist, and the nullvector is just an arbitrary pick among them. Nevertheless, we found that the directions in the case of unrestricted eye movements were always balanced.

IV. TEMPLATE MODEL

The template model and the velocity gain field model both rely on templates tuned to heading and a specific component of rotation. But, as to make each local contribution to a template invariant to the distances of points, the velocity gain field explicitly assumes only the component of flow along the circular structure is measured, while the template approach (Perrone & Stone, 1994) selects the maximum response of various motion sensors. Does the template approach predict circular receptive fields as well?

IV.I. Receptive Fields in Template Model

In the template approach, at each location not one motion sensor is read-out, but the most active one in a set of motion sensors tuned to different depth planes but same preferred heading and rotation. Each motion sensor has a preferred motion that is the vector sum of a radial vector, expected from a translating point on a certain depth plane, combined with a motion vector expected from the template's preferred rotation (Figure 8a). As one can see, the expected vector sums C_i at one specific location, are constrained by a line that runs parallel to the radial line. Motion parallel to this constraint line will only change which sensor is maximal active, but not lead to a change in maximal activity (unless the motion lies outside the range of each motion sensor). Only motion perpendicular to the constraint line will change the maximal activity. This motion is directed along the circle centered on the preferred heading, and equals the expected motion from the template's preferred rotation (R), taken along the circle centered on the preferred heading (C_c).

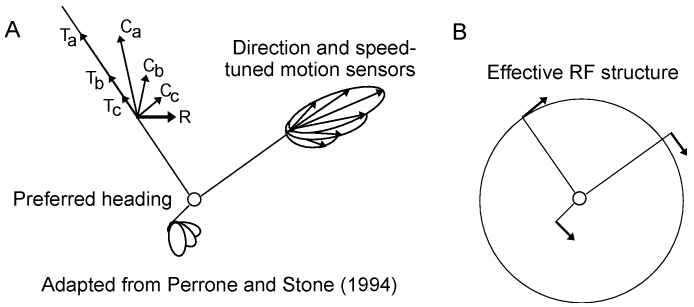

Figure 8. a) Each template sums the responses of the most active sensor at each location. This most active motion sensor is selected from a pool of sensors tuned to different depth planes (Ca, Cb, etc). These vectors are the vector sums of preferred rotation component R and translational components Ta, Tb, etc. b) At each location the effective motion vector driving the template is tangent to a circle, centered on the template's preferred heading.

Note, the most active motion sensors need not be directed along heading-centered circles. This is clearly the case for the pure translation template. But, also for a template with a preferred component of rotation, the contributing motion sensor need not be oriented along the circle, for instance if the expected rotational motion vector is not tangent to the circle. Then, the local contribution would be determined by the directional tuning rather than the velocity tuning of the most active sensor. Still, the effective motion vector that drives the template's output is oriented along a circle centered on the template's preferred heading (Figure 8b). Whereas the velocity gain field model leaves unspecified how the velocity and direction tuning to motion along the circle might be accomplished at MT level, the selection of maximum activity from a set of constrained sensors, as proposed by the template model, might be a way to realise such tuning.

V. DISCUSSION

V.I. Heading-centered Circular RF Structures: Intuitive or Counterintuitive?

We looked at the structure of receptive fields for flow analysis in three models for heading detection. The models apply different methods to solve the heading. Nevertheless, we find in all three cases the directions of preferred motion to be constrained along circles centered on the heading.
Circular RFs for heading detection seem rather counterintuitive, for the flow expected from ego-translation is radial. Why would a circular structure be

optimal to detect heading? The important point to realise here is that only a deviation from expected heading is of interest. Thus, only the component of translation perpendicular to expected translation really is of importance to sense heading, not the component in the expected heading direction. As the components in the expected heading direction are radial, what is left to be analysed are components of flow along the circles centered on the expected heading.

How can circular RFs still measure heading? This can be understood by examining the effects of components of translational and rotational flow separately. As shown in Figure 9, a heading-centered circular RF only measures the translational flow caused by translation perpendicular to the preferred heading. By measuring the evidence for zero motion along its preferred circular structure, a neuron can sense a deviation from its preferred heading direction, while not being too sensitive to variations in translational speed along the preferred heading and distances of points.

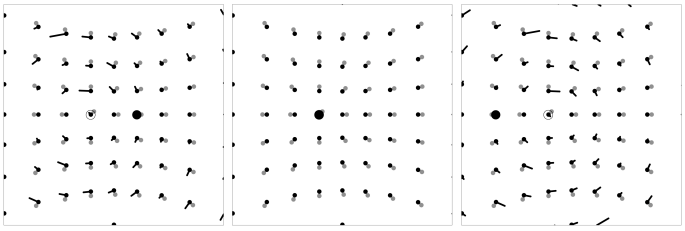

Figure 9. Circular component of flow (solid inner vectors) resulting from pure translation through a 3D cloud in three different directions (filled circle in each plot), measured along the preferred circular RF structure (gray outer vectors) centered on preferred heading (open circle).

Circular receptive field structures could explain why area MST is found to be not only selective for expanding motion patterns, but also has a significant proportion of cells are selective to rotation patterns (Duffy & Wurtz, 1991a, b; Lappe et al., 1996; Tanaka et al., 1989; Tanaka & Saito, 1989). The link between selectivity for circular flow structures and heading detection mechanisms also suggests that testing selectivity for expanding motion might be a bad indicator for determining a cell's preferred heading. This point has been noted before, as MST seems to be systematically tuned to the focus of rotation, exactly like model neurons the population model (Lappe et al., 1996). Another way to test for circular RF structure might be to look at sensitivity to the variations in translational speed or in the speed gradient, when radial flow is centered on the cell's preferred heading. Indeed, early studies suggest that expansion cells are not sensitive to the speed gradient (Tanaka et al., 1989; Orban, Lagae & Raiguel, 1995) or speed itself (Duffy & Wurtz, 1991a). Recent studies do suggest speed sensitivity in MST (Duffy & Wurtz, 1997, Upadhyay, Page & Duffy, 2000) and area 7a (Phinney & Siegel, 2000). However, critical would still be to know whether the expanding motion

was presented exactly centered on the cell's preferred heading.

V.II. RF Structures and Rotation Invariance

Given neurons measure the evidence for zero-motion along their circular structure, how do they acquire invariance to rotation and what substructures might arise?

In both the velocity gain field model (Beintema & van den Berg, 1998), as well as the template model (Perrone & Stone, 1994), the evidence for zero-motion along the circular structure is measured by a pure translation template. Its activity ($O_{\mathbf{t}}$ in the velocity gain field model) is computed by summing the outputs of motion sensor, where each local motion sensors is oriented along the circular structure and assumed to be tuned to zero-motion. However, because each pure translation template will be influenced by a component of rotation, some trick must be applied to assure the correct template is maximal active.

In the template model, the rotation problem is simply solved by assuming an array of templates that includes all possible combinations of two-dimensional heading and three-dimensional rotations. Such approach requires many rotation-tuned templates per rotation axis, although one can reduce the dimensions when assuming the eye movements are restricted (Perrone & Stone, 1994). An alternative solution to the rotation problem is used in the velocity gain field approach (Beintema & van den Berg, 1998). Any change in activity of a pure translation template $O_{\mathbf{t}}$ due to a component of rotation is compensated by subtracting an appropriate derivative template activity, multiplied by a measure of the evidence for rotation about that axis $\left[\right]$, i.e. $\left[\right]\partial O/\partial R$. The range of rotation velocities is limited by the preferred rotation of the templates, but can be expanded by assuming also pairs tuned to larger rotation velocities.

Thus, both the template and velocity gain field model predict templates specially tuned to heading and zero-preferred rotation (zero-preferred motion along circles). Their receptive field would consist of motion detectors directed along the circular structure, but with zero-preferred motion. But, even more abundantly represented might be templates tuned to heading and a component of rotation about a given axis, especially about an axis perpendicular to the heading, giving rise of *bi-circular* RF structures. Units tuned to rotation about the heading axis would have a *uni-circular* RF structure.

The population model acquires invariance to rotation and depths of points in a different way. Given the locations (image coordinates) of motion inputs to the neuron u, the subspace algorithm is used to generate sets of preferred motion vectors $\mathbf{v}_i$ whose summed inproducts with the presented motion vectors must always be zero $\sum_{i=1}^{m} \mathbf{v}_i \cdot \square_i = 0$ (i.e. the residual function $R(\mathbf{T})$ when the preferred heading is presented. The subspace algorithm splits the flow

equations into a part related to translation and a part related to the rotation. The requirement of invariance to translational speed and distances of points constrains all preferred motion vectors to lie on along circles centered on the preferred heading. Given that the sum of vector inproducts along the circles must be zero also in case of rotation, this additionally constrains the directions (clockwise or counterclockwise) and magnitudes of preferred motion vectors.

Taken the results from our analysis, we can interpret how the RF structure plays its role in obtaining invariance to rotation. The simplest case occurs for arrangements in local pairs, in which case the preferred motion vectors of pairs were found to be opponent and equal of magnitude. Such arrangement evidently will exclude any contribution from rotational flow to the residual function, because rotation causes two point to move exactly in same direction at same speed. Since one motion vector excites one of the motion sensors, and the same motion inhibits the response of the other motion sensor, their contributions exactly cancel. That the model is able to detect heading for such local motion-opponent pairs, relies on the fact differential motion will be presented as soon as the heading deviates from the preferred heading. Obviously, such local pair arrangements makes heading detection rely on the presence of depth differences along the same visual direction (edges, etc.).

For more spatially separated motion inputs, the results for restricted eye movement results are helpful to interpret how invariance to rotation is obtained, for then only one possible axis of rotation was assumed. In that case, we found that the preferred motion magnitude varied sinusoidally as function of the position on the circles (Figure 5), such that is small when the motion vector expected from rotation is large, and vice versa. This way the sum of two motion responses will cancel during rotation about the vertical axis.

More difficult to analyse is the receptive field structure for unrestricted eye movements, in which case a minimum of four motion vectors is required as input to a u_{jl} neuron. The receptive field structure turned out to be opponent on average. This can be interpreted as a consequence of assumed invariance to rotation about all possible axes. Because the motion directions are balanced in clockwise and counterclockwise direction, flow caused by a rotation about the line of sight does not give a net motion input to the residual function. Also, because the four vectors are balanced vertically and horizontally, the contributions of flow caused by rotation perpendicular to the heading axis also cancel.

In summary, we find that the population arrives at rotation-invariance in a way essentially different from template approaches. It relies on zero-motion parallax detection, rather than on zero motion detection as assumed in the velocity gain field model or template model. This difference leads to different expected substructures within the circular RF. Receptive fields meant to measure zero uniform motion require additional RFs that provide estimates of ego-rotation.

V.III. Opponent-motion RF Structures

Especially, when the motion inputs are arranged in pairs of local neighbouring motion inputs, a clear opponent motion RF structure emerges in the population model. This property of the subspace algorithm was also noted by Heeger and Jepson (1992a), who proposed a center-surround motion-opponent structure to measure heading. The population model's reliance on motion-parallax to obtain rotation invariant heading estimates has great analogue to Longuet-Higgins & Prazdny's (1980) original use of differential motion parallax. Their approach exploited the fact that local difference motion vectors are constrained to be oriented radially and intersect at the heading direction. As this approach relies on the presence of motion parallax in one visual direction, it requires scenes with depth edges. The differential motion approach can be improved by computing motion differences within a larger visual area, therefore not requiring the presence of depth edges (Rieger & Lawton, 1985; Hildreth, 1992; Royden, 1997). Indeed, a physiological implementation of this idea assumes the local motion-opponency outputs are summed by a MST-like template which measure the evidence for non-zero differential motion along the radial structure centered on the cell's preferred heading (Royden, 1997). The downside of exploiting motion differences this way, however, is that radial flow detectors are still sensitive to variations in distances of points or to translational velocity.
In contrast, the population model arrangement in local motion-opponent pairs analyses the heading by MST-like cells that detect the evidence for *zero motion-opponency* along their preferred circular structure. This approach is invariant to the translational velocities and distances of points. In that respect, the population model approach is an improvement over traditional motion-parallax theories. Furthermore, the opponent character of pairs in the population model is not restricted to locally near sensors, but is also seen for motion sensors further apart.

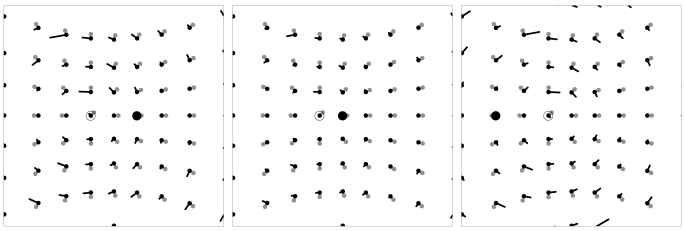

Figure 10. Circular component of flow (solid inner vectors) resulting from rotation combined with observer translation in three different directions (filled circle in each plot), compared with the preferred bi-circular RF structure (gray outer vectors) centered on the preferred heading (open circle).

Do the receptive fields of templates also exploit motion-parallax by pairs of opponent-motion sensors? The derivative template response, computed by locally subtracting the responses of a pair of templates with opposite preferred rotation, does predict such an opponent structure. However, this local subtraction of motion activities is meant to give a local estimate of the rotation, not an estimate of a local motion difference. Thus, motion parallax is considered noise by these templates.

The velocity gain field model, however, included an extension to allow pure visual solutions (Beintema & van den Berg, 1998) that might be the analogue for the detection of zero-motion parallax. The added feature was the suppression of those $H_{\mathbf{t}}$ templates that use false estimates of the rotation. Such wrong estimates occur for derivative template activities that are contaminated by components of translational flow along their preferred circular structure. As shown in Figure 10 this occurs for non-preferred headings. To get around this problem, the authors theorised that some measure of variance in the presented flow along the circular structure due to motion parallax might be exploited for suppression in case of a non-preferred heading. To this end they used the variance of local estimates of the flow along the circular structure, each scaled with the preferred local flow of a rotation-tuned template. This measure of variance in local rotational gain is not sensitive to rotation about the preferred axis, but does rise with increased motion parallax along the preferred circular structure. Suppressing the output of a template $H_{\mathbf{t}}$ when the variance is high due to the presence of motion parallax seems similar to reducing the response of neuron u_{jl} in the population model when it measures evidence for non-zero-motion parallax. Therefore, this extension to the velocity gain field model might also be based on a motion-opponent structure that truly measures differences in motion.

In summary, motion opponency seems to emerge in models encoding heading at the level of MST as well, except for the template approach (Perrone & Stone, 1994) which does not exploit the use of motion-parallax cues. So far opponent-motion detectors have only been found at the level of MT cells. Our analysis suggests to look for such opponent-motion structures, at the level of at a higher level as well, be it along circular RF structures.

V.IV. Bi-circular RF Structures

A typical substructure in circular receptive fields predicted by the velocity gain field model and the template model is bi-circularity. Interestingly, for the restricted version of the population model that assumes tracking eye movements, we were able to construct a *uni-circular* RF and *bi-circular* RF for specific spatial arrangements of the motion inputs. In terms of velocity gain field templates, these two substructures would be optimally tuned to a rotation about the line of sight, and about an fronto-parallel axis parallel to the heading axis, respectively. Such sensitivity to rotation is

perfectly in line with the assumption of tracking eye movements, because this only assumes invariance for rotation about the axis perpendicular to the heading axis and the line of sight. However, for unrestricted eye movements, we found no possible arrangement of points that would fit a *bi-circular* or *uni-circular* RF. Therefore, these substructures are unlikely an essential feature of the population model.

Bi-circular receptive fields might play a role as visual rotation estimators. Visual estimates of rotation can only be reliable made at the level of global flow analysis. Such visual rotation estimates could, for instance, be important to gauge extra-retinal signals about rotation of the eye. Bi-circular RFs would also allow the use extra-retinal signals at a more global level of motion analysis (Beintema & van den Berg, 1998). The population model can also be extended to use extra-retinal signals, but at a more local level (Lappe, 1998). So far, clear evidence for an interaction between visual and extra-retinal signals has only been found at the level of MST responses (Bradley, Maxwell, & Andersen, 1996; Shenoy, Bradley & Andersen, 1999). Moreover, psychophysical experiments on perceived heading suggest that extra-retinal signals must interact beyond the level at which neurons analyse the local flow (Beintema & van den Berg, 2001). A direct comparison of the extra-retinal and visual estimates of rotation allows one model (Beintema & van den Berg, 1998) to explain on one side the benefit of extra-retinal signals during real eye rotations for judging heading when motion parallax cues are absent (Royden et al., 1992), and on the other side the benefit of motion-parallax cues during simulated eye rotation (van den Berg, 1992; Warren & Hannon, 1990).

Thus, bi-circular RF structures seem important substructures of receptive fields to look for. MST responses to uni-circular motion, where the focus of rotation is presented outside the visual field (Duffy & Wurtz 1995) (Duffy & Wurtz, 1995; Graziano et al., 1994), might be in line with bi-circular RFs, because then only part of uni-circular flow matches bi-circular flow. But whether MST cells truly have such substructures still remains to be investigated.

V.V. Conclusion

The analysis of the receptive field structure in neurophysiologically inspired models provides new insights into how the brain might detect heading most effectively. The most important conclusion is that the models predict a circular, not radial, receptive field, centered on the neuron's preferred heading. Different strategies to arrive at rotation invariance lead to different predicted substructures. To exploit motion parallax cues, detectors might be organised in motion-opponent pairs and measure the evidence for null motion-opponency along the circular structure. Explicit representations of visual evidence for rotation would predict bi-circular structures. Seeking evidence for circular and more refined structures offer challenging directions

for future research.

Acknowledgements

ML is supported by the German Science Foundation, the German Federal Ministry of Education and Research, the HFSP and the EC Ecovision Project. AB and JB are supported by NWO and the HFSP.

REFERENCES

Allman, J., Miezin, F., & McGuinness, E. (1985). Stimulus specific responses from beyond the classical receptive field: Neurophysiological mechanisms for local-global comparisons in visual neurons. *Annual Review of Neuroscience, 8*, 407-430.

Andersen, R.A., Essick, G.K., & Siegel, R.M. (1985). Encoding of spatial location by posterior parietal neurons. *Science, 230* (4724), 456-458.

Beintema, J.A., & van den Berg, A.V. (1998). Heading detection using motion templates and eye velocity gain fields. *Vision Research, 38* (14), 2155-2179.

Beintema, J.A., & van den Berg, A.V. (2001). Pursuit affects precision of perceived heading for small viewing apertures. *Vision Research, 41* (18), 2375-2391.

Beintema, J.A., van den Berg, A.V., & Lappe, M. (2002). Receptive field structure of flow detectors for heading perception. In: T.G. Dietterich, S. Becker, & Z. Ghahramani (Eds.), *Neural Information Processing Systems,* 14, MIT Press, Cambridge, MA.

Bradley, D.C., Maxwell, M., Andersen, R.A., Banks, M.S., & Shenoy, K.V. (1996). Mechanisms of heading perception in primate visual cortex. *Science, 273* (5281), 1544-1547.

Britten, K.H., & van Wezel, R.J. (1998). Electrical microstimulation of cortical area MST biases heading perception in monkeys. *Nature Neuroscience, 1* (1), 59-63.

Colby, C.L., Duhamel, J.R., & Goldberg, M.E. (1993). Ventral intraparietal area of the macaque: anatomic location and visual response properties. *Journal of Neurophysiology, 69* (3), 902-914.

Duffy, C.J., & Wurtz, R.H. (1991a). Sensitivity of MST neurons to optic flow stimuli. I. A continuum of response selectivity to large-field stimuli. *Journal of Neurophysiology, 65* (6), 1329-1345.

Duffy, C.J., & Wurtz, R.H. (1991b). Sensitivity of MST neurons to optic flow stimuli. II. Mechanisms of response selectivity revealed by small-field stimuli. *Journal of Neurophysiology, 65* (6), 1346-1359.

Duffy, C.J., & Wurtz, R.H. (1995). Response of monkey MST neurons to optic flow stimuli with shifted centers of motion. *Journal of Neuroscience, 15* (7), 5192-5208.

Duffy, C.J., & Wurtz, R.H. (1997). Medial superior temporal area neurons respond to speed patterns in optic flow. *Journal of Neuroscience, 17* (8), 2839-2851.

Graziano, M.S., Andersen, R.A., & Snowden, R.J. (1994). Tuning of MST neurons to spiral motions. *Journal of Neuroscience, 14* (1), 54-67.

Grigo, A., & Lappe, M. (1999). Dynamical use of different sources of information in heading judgments from retinal flow. *Journal of the Optical Society of America A Opt Im Sci Vis, 16* (9), 2079-2091.

Hatsopoulos, N.G., & Warren, W.H., Jr. (1991). Visual navigation with a neural network. *Neural Networks, 4* (3), 303-318.

Heeger, D.J., & Jepson, A. (1990). Subspace methods for recovering rigid motion, II: theory. *Technical Report,* RBCV-TR-90-36 (Dept of Computer Science, University Toronto.

Heeger, D.J., & Jepson, A. (1992a). Recovering observer translation with center-surround motion-opponent mechanisms. *Investigative Ophthalmology & Visual Science Supplement, 32*, 823.

Heeger, D.J., & Jepson, A. (1992b). Subspace methods for recovering rigid motion I: algorithm

and implementation. *International Journal of Computer Vision, 7*, 95-117.
Hildreth, E.C. (1992). Recovering heading for visually-guided navigation. *Vision Research, 32* (6), 1177-1192.
Lappe, M. (1998). A model of the combination of optic flow and extraretinal eye movement signals in primate extrastriate visual cortex. *Neural Networks, 11*, 397-414.
Lappe, M. (2000). Computational mechanisms for optic flow analysis in primate cortex. *International Review of Neurobiology, 44*, 235-268.
Lappe, M., Bremmer, F., Pekel, M., Thiele, A., & Hoffmann, K.P. (1996). Optic flow processing in monkey STS: a theoretical and experimental approach. *Journal of Neuroscience, 16* (19), 6265-6285.
Lappe, M., & Rauschecker, J.P. (1993a). Computation of heading direction from optic flow in visual cortex. In: C.L. Giles, S.J. Hanson, & J.D. Cowan (Eds.), *Advances in Neural Information Processing Systems,* 5 (pp. 433-440). San Mateo, CA: Morgan Kaufmann.
Lappe, M., & Rauschecker, J.P. (1993b). A neural network for the processing of optic flow from ego-motion in man and higher mammals. *Neural Computation, 5*, 374-391.
Lappe, M., & Rauschecker, J.P. (1995). Motion anisotropies and heading detection. *Biological Cybernetics, 72* (3), 261-277.
Longuet-Higgins, H.C., & Prazdny, K. (1980). The interpretation of a moving retinal image. *Proceedings of the Royal Society of London B Biol Sci, 208* (1173), 385-397.
Orban, G.A., Lagae, L., Raiguel, S., Xiao, D., & Maes, H. (1995). The speed tuning of medial superior temporal (MST) cell responses to optic-flow components. *Perception, 24* (3), 269-285.
Perrone, J.A. (1992). Model for the computation of self-motion in biological systems. *Journal of Neurophysiology, 9* (2), 177-194.
Perrone, J.A., & Stone, L.S. (1994). A model of self-motion estimation within primate extrastriate visual cortex. *Vision Research, 34* (21), 2917-2938.
Phinney, R.E., & Siegel, R.M. (2000). Speed selectivity for optic flow in area 7a of the behaving macaque. *Cerebral Cortex, 10* (4), 413-421.
Read, H.L., & Siegel, R.M. (1997). Modulation of responses to optic flow in area 7a by retinotopic and oculomotor cues in monkey. *Cerebral Cortex, 7* (7), 647-661.
Rieger, J.H., & Lawton, D.T. (1985). Processing differential image motion. *Journal of the Optical Society of America A, 2* (2), 354-360.
Royden, C.S. (1997). Mathematical analysis of motion-opponent mechanisms used in the determination of heading and depth. *Journal of the Optical Society of America A, 14* (9), 2128-2143.
Royden, C.S., Banks, M.S., & Crowell, J.A. (1992). The perception of heading during eye movements. *Nature, 360* (6404), 583-585.
Shenoy, K.V., Bradley, D.C., & Andersen, R.A. (1999). Influence of gaze rotation on the visual response of primate MSTd neurons. *Journal of Neurophysiology, 81* (6), 2764-2786.
Tanaka, K., Fukada, Y., & Saito, H.A. (1989). Underlying mechanisms of the response specificity of expansion/contraction and rotation cells in the dorsal part of the medial superior temporal area of the macaque monkey. *Journal of Neurophysiology, 62* (3), 642-656.
Tanaka, K., & Saito, H. (1989). Analysis of motion of the visual field by direction, expansion/contraction, and rotation cells clustered in the dorsal part of the medial superior temporal area of the macaque monkey. *Journal of Neurophysiology, 62* (3), 626-641.
Upadhyay, U.D., Page, W.K., & Duffy, C.J. (2000). MST responses to pursuit across optic flow with motion parallax. *Journal of Neurophysiology, 84* (2), 818-826.
van den Berg, A.V. (1992). Robustness of perception of heading from optic flow. *Vision Research, 32* (7), 1285-1296.
van den Berg, A.V., Beintema, J.A., & Frens, M.A. (2001). Heading and path percepts from visual flow and eye pursuit signals. *Vision Research, 41* (25-26), 3467-3486.
van Wezel, R.J., & Britten, K.H. (2002). Multiple uses of visual motion. The case for stability in sensory cortex. *Neuroscience, 111* (4), 739-759.
Warren, W.H., Jr., & Hannon, D.J. (1990). Eye movements and optical flow. *Journal of the Optical Society of America A, 7* (1), 160-169.